Electrostatic potentials in the downward auroral current region

Jörgen Vedin and Kjell Rönnmark

Department of Physics, Umeå University, Umeå, Sweden

[1] Assuming a fixed ion density, adiabatic electron motion, and quasi-neutrality, we use the stationary Vlasov equation to derive the self-consistent potential in an auroral flux tube that carries downward current. Our model predicts downward electric fields $\sim$5 mV/m at an altitude near 2000 km, and around 4000 km the potential reaches $\sim$2.5 kV. A weak upward electric field at high altitudes reduces the potential, and the potential difference between the ionosphere and magnetosphere is much smaller.

Citation: Vedin, J., and K. Rönnmark (2005), Electrostatic potentials in the downward auroral current region, *J. Geophys. Res.*, *110*, A08207, doi:10.1029/2005JA011083.

1. Introduction

[2] The auroral current circuit plays a crucial role in the transfer of energy and momentum between the magnetosphere and the ionosphere. Although upward and downward currents should be equally important for magnetosphere-ionosphere coupling, the upward current region has received much more attention, probably because of its association with visible auroral displays. There have been numerous studies of upward auroral currents and the acceleration of precipitating auroral electrons by field-aligned electric fields. There is a well-established current-voltage relation [*Knight*, 1973], applicable to stationary upward currents. Many numerical simulations, based on fluid plasma models, have been done to study the dynamics of electron acceleration by Alfvén waves [e.g., *Goertz and Boswell*, 1979; *Lysak and Dum*, 1983; *Streltsov et al.*, 1998; *Tikhonchuk and Rankin*, 2000; *Rönnmark and Hamrin*, 2000]. The relation between the stationary, electrostatic, kinetic models and the dynamic fluid models have recently been investigated [*Tikhonchuk and Rankin*, 2002; *Lysak and Song*, 2003; *Vedin and Rönnmark*, 2004, 2005]. In comparison, there have been very few attempts to develop theoretical models for the downward current region, but satellite observations indicate that the physics of the downward auroral current region is very dynamic, complex, and interesting [e.g., *Marklund and Karlsson*, 2001; *Lynch et al.*, 2002; *Andersson et al.*, 2002]. In this article we will discuss a model that can describe some fundamental properties of downward auroral currents and potentials.

[3] There are several different timescales that are important when constructing a model of fields and currents in auroral flux tubes. The fastest by far is the inverse plasma frequency, which characterizes the time it takes to establish quasi-neutrality over distances of a few Debye lengths. Since we will consider frequencies much lower than the plasma frequency and length scales much longer than the Debye length, we can safely assume the plasma to be quasi-neutral. Another important timescale is determined by the time it takes electrons with typical velocity V_e to go through a flux tube of length L_z, which is $\tau_e \sim L_z/V_e$. If the electric field can be considered stationary during times $\sim\tau_e$ the electron distribution can be assumed to satisfy the stationary Vlasov equation. A comparable timescale is determined by the propagation time of an Alfvén wave along the flux tube, or $\tau_A \sim L_z/V_A$, where V_A is a typical Alfvén velocity. On timescales shorter than τ_A, but longer than the inverse of the ion gyrofrequency, the dynamics is dominated by Alfvén waves. The ion density will vary on a timescale τ_i, which is much longer than τ_e since the ions are much heavier. Typically, we have $\tau_A \sim \tau_e$ 10 s and $\tau_i \gtrsim$ 100 s. In this study we will consider fields and currents that vary on timescales τ that satisfy $\tau_A \sim \tau_e \lesssim \tau \lesssim \tau_i$. This implies that the perpendicular ion polarization currents associated with Alfvén waves can be neglected, and we may assume that the field-aligned electron current is conserved. Since the electrons experience an essentially stationary potential while they move through the flux tube, we can also assume that the electron density is roughly in equilibrium with the electrostatic potential while the ion density is more or less fixed.

[4] Steady state models that describe the low-altitude ($\lesssim$1 R_E) part of the downward current region have been studied by *Jasperse* [1998] and *Jasperse and Grossbard* [2000]. They derive a set of multimoment fluid equations, including the effects of quasi-linear diffusion of the particles in velocity space. From these equations they can derive equilibrium altitude profiles of, for example, the field-aligned electric field and the particle temperatures. The solutions they obtain are compared with observations from the S3-3 and Freja satellites. These studies are in several ways complemented by the model we present here. Our model extends out to 8.6 R_E from the ionosphere and is limited to times when the ion density has not adjusted to variations in the current and

potential. Rather than comparing with a set of observations, our aim in this study is to elucidate some of the mechanisms believed to be important on these timescales, using the simplest model that contains the relevant physics. We will also vary the boundary conditions that determine the current in order to obtain a current-voltage relation.

[5] The current-voltage relationship in the downward auroral current region was studied by *Temerin and Carlson* [1998]. The main idea behind the Temerin-Carlson model is to use the continuity equation to determine how the density of the ionospheric electrons depends on the current and to find a potential that reduces the density of magnetospheric electrons by the same amount to keep the plasma quasi-neutral. At high altitudes they keep the ion density fixed, but it is allowed to vary with the current at altitudes below 1 R_E. Although the study of *Temerin and Carlson* [1998] contained some rather crude approximations and was rather briefly presented, their ideas have been an important inspiration for our work.

[6] This study will be based on accurate density calculations, taking into account the adiabatic electron trajectories in an inhomogeneous magnetic field and an electrostatic potential that is self-consistently determined by the requirement of quasi-neutrality. In sections 2 and 3, we discuss the boundary and initial conditions pertinent to our model. Section 4 describes the density calculations, why quasi-neutrality forces us to modify the boundary conditions, and how the potential is calculated. The results are presented in section 5 and discussed in section 6.

2. Boundary Conditions

[7] We will describe the flux tube by a one-dimensional model, using a magnetic field aligned coordinate z, with $z = 0$ in the equatorial plane and $z = z_F$ at the boundary in the ionospheric F layer. The magnetic field will then be denoted $B = B(z)$. The distribution function f_F of upgoing electrons at the ionospheric boundary of the flux tube in the F layer of the ionosphere is

$$f_F(v) = N_F \left(\frac{m}{2\pi T_F}\right)^{3/2} \exp\left[-\frac{v^2}{v_F^2}\right], \qquad (1)$$

where the density is $N_F = 10^{11}$ m^{-3} and the temperature $T_F = 1$ eV defines the thermal velocity v_F by $T_F = mv_F^2/2$ with m denoting the electron mass.

[8] Close to the equatorial plane we assume that there is a generator region, which cannot be described by our electrostatic, kinetic model. The boundary of the generator region is taken to be at z_G. Within the generator, at $z < z_G$, the field-aligned current is diverted into a perpendicular current carried by ions. Since we consider only electron dynamics, and the field-aligned current is automatically conserved within our model, we cannot expect to properly describe the generator processes. Hence the model developed below applies only to $z > z_G$.

[9] The current in the flux tube is determined by conditions within the generator region. It is then not obvious that the boundary conditions at z_G should be constant, independent of the current. However, as a first attempt,

we will assume that the distribution function f_G of downgoing electrons at this boundary is

$$f_G(v) = N_G \left(\frac{m}{2\pi T_G}\right)^{3/2} \exp\left[-\frac{v^2}{v_G^2}\right], \qquad (2)$$

with $mv_G^2/2 = T_G = 1$ keV and a constant $N_G = 5 \times 10^5$ m^{-3}. As will be seen later, we will be forced to reconsider the assumption of a constant N_G, since it turns out that this assumption leads to inconsistent boundary conditions.

3. Initial Conditions

[10] A study of how the electrostatic potential depends on the downward current should start from a well-defined initial state. The natural starting point is a current-free flux tube. In this section, we will determine the ambipolar potential that gives zero current and define the plasma properties in this initial state.

[11] An auroral flux tube would in the absence of any field-aligned electric fields carry a substantial downward current. Assuming that no ionospheric electrons come back down the field line, the current density at the ionospheric boundary can be calculated by integrating the distribution function over the hemisphere of upgoing velocities, which yields

$$j_{IF} = \frac{eN_F}{2\sqrt{\pi}} v_F. \qquad (3)$$

Here, we have introduced $-e$ as the electron charge. Magnetospheric electrons that reach the ionospheric boundary of the flux tube are lost into the atmosphere. The hemisphere of downgoing velocities is filled with magnetospheric electrons at the ionospheric boundary, and the upward current density carried by magnetospheric electrons can be calculated as

$$j_{MF} = -\frac{eN_G}{2\sqrt{\pi}} v_G. \qquad (4)$$

In the absence of field-aligned electric fields, the ionospheric electrons would completely dominate, yielding a total downward current density at the ionosphere $j_F = j_{MF} + j_{IF} \sim 25$ mA/m^2, which is several orders of magnitude larger than the field-aligned currents observed in the auroral region. To prevent this outflow of ionospheric electrons, an ambipolar electric field is required.

[12] The ions are gravitationally bound to the Earth, and any deviations from quasi-neutrality will cause an ambipolar electric field that stops the electrons from escaping up the field line. We will introduce a function $\Phi(z)$ to describe the potential that generates the ambipolar electric field $E_a = -e^{-1}\partial_z\Phi$. Notice that to keep the notations in the following derivations simple, we include e in the potential and write the potential and temperatures in energy units. A model for the ambipolar electric field can be found by balancing the gravitational force on the ions, which is $\propto B^{2/3}$, by an electric field at low altitudes, $z \geq z_a$, and neglecting gravitation for $z < z_a$. Notice that a higher ion temperature makes gravitation negligible at

lower altitudes or larger z_a. This suggests the simple model

$$\Phi(z) = \begin{cases} \Phi_a \dfrac{B^{1/3}(z) - B_a^{1/3}}{B_F^{1/3} - B_a^{1/3}}, & \text{if } z \geq z_a; \\ 0, & \text{if } z < z_a. \end{cases} \qquad (5)$$

Here $\Phi_a = \Phi(z_F)$ is the total ambipolar potential drop, $B_F = B(z_F)$, and $B_a = B(z_a)$. The ambipolar potential drop Φ_a is determined by solving the equation

$$j_{IF}(\Phi_a) + j_{MF}(\Phi_a) = 0, \qquad (6)$$

where

$$j_{IF}(\Phi_a) = \frac{eN_F v_F}{2\sqrt{\pi}} \frac{B_F}{B_a} \left[1 - \left(1 - \frac{B_a}{B_F} \right) e^{-\frac{\Phi_a/T_F}{B_F/B_a - 1}} \right] e^{-\frac{\Phi_a}{T_F}} \qquad (7)$$

and

$$j_{MF}(\Phi_a) = -\frac{eN_G v_G}{2\sqrt{\pi}} \frac{B_F}{B_a} \left[1 - \left(1 - \frac{B_a}{B_F} \right) e^{-\frac{\Phi_a/T_G}{B_F/B_a - 1}} \right]. \qquad (8)$$

Having specified the potential $\Phi(z)$, we can find the electron density in the initial state, using methods described in the next section. Assuming quasi-neutrality, we take the ion density $n_i = n_i(z)$ to be equal to the electron density in this state with zero net current. We denote this initial magnetospheric electron density n_{Ma} and the corresponding ionospheric electron density n_{Ia}.

4. Model

[13] If required by changing boundary conditions, the electrons will on timescales of a few seconds establish a new quasi-neutral equilibrium with a nonzero current and and a new electrostatic potential $\phi = \phi(z)$. On the timescale τ_e, related to the time it takes an electron to travel between the boundaries of the flux tube, the density of the heavy ions will not change significantly. Hence we will consider the ion density $n_i(z)$ to be a fixed given function, which the potential and electrons adjust to. This does not exclude that the ion density may change on longer timescales (100 s) than those required for the electrons to establish a potential consistent with quasi-neutrality.

[14] To obtain a downward current, we must modify the potential. We assume that the potential $\phi(z)$ has a global minimum at a point z_0 and choose $\phi(z_0) = 0$. As long as the potential satisfies

$$\phi(z) \geq \phi_F \frac{B(z) - B_0}{B_F - B_0}; \qquad z > z_0, \qquad (9)$$

where $\phi_F = \phi(z_F)$ and $B_0 = B(z_0)$, we can easily generalize equation (7) for the current carried by ionospheric electrons to

$$j_{IF}(\phi_F) = \frac{eN_F v_F}{2\sqrt{\pi}} \frac{B_F}{B_0} \left[1 - \left(1 - \frac{B_0}{B_F} \right) e^{-\frac{\phi_F/T_F}{B_F/B_0 - 1}} \right] e^{-\frac{\phi_F}{T_F}}. \qquad (10)$$

We see that a reduction of the ionospheric potential ϕ_F corresponds to an increase in the downward current. A quasi-neutral solution with a downward current is then obtained by choosing a $\phi_F < \Phi_a$ and adjusting $\phi(z)$ along the rest of the field line to make the electron density consistent with $n_i(z)$.

4.1. Electron Density

[15] The calculation of the electron density in an auroral flux tube with given potential and electron distributions at the boundaries has been previously discussed by *Janhunen* [1999] and [*Vedin and Rönnmark*, 2004]. To calculate the densities, we write the velocity distributions as functions of the energy

$$H = \frac{mv^2}{2} - \phi = \frac{mv_z^2}{2} + \mu B - \phi \qquad (11)$$

and the magnetic moment

$$\mu = \frac{mv_\perp^2}{2B}. \qquad (12)$$

Transforming to these new variables, which are constant along the electron trajectories, the Vlasov equation can easily be solved as described by *Vedin and Rönnmark* [2004]. This determines the distribution function within the flux tube, given the boundary conditions in equations (1) and (2). The integrals of the distribution function that give the electron density can be written

$$\frac{B}{2\sqrt{\pi}} \frac{N}{T^{3/2}} \int_{H_{\min}}^{\infty} e^{-H/T} dH \int_0^{\mu_{\max}} \frac{d\mu}{\sqrt{H + \phi - \mu B}}$$
$$= \frac{1}{\sqrt{\pi}} \frac{N}{T^{3/2}} \int_{H_{\min}}^{\infty} e^{-H/T}$$
$$\cdot \left[\sqrt{H + \phi} - \sqrt{H + \phi - \mu_{\max}(z, H)B} \right] dH, \qquad (13)$$

where $\mu_{\max}(z, H)$ is the maximum μ value for a given z as a function of H, and $H_{\min}$ is the H value at $\mu = 0$ for the desired integration boundary. To determine the limits of integration ($\mu_{\max}(z, H)$ and $H_{\min}$), we use the general method described by *Vedin and Rönnmark* [2004]. Introducing a set of grid points $z_k = z_G + k\Delta z$, the integration boundary $\mu_{\max}(z, H)$ is approximated by a finite number of straight line segments. For example, at $z = z_2$, $\mu_{\max}(z, H)$ limits the shaded integration area as in Figure 1. This figure clearly demonstrates that if $\phi(z)$ is increasing sufficiently fast, the integration area at z_k may depend also on the potential at $z < z_k$.

[16] The densities can then be written as a sum of integrals of the generic form

$$I(H_1, H_2, \alpha, \beta) = \frac{1}{\sqrt{\pi}} \frac{N}{T^{3/2}} \int_{H_1}^{H_2} e^{-H/T} \sqrt{\alpha H + \beta} \, dH$$
$$= \frac{N}{2} \left[\sqrt{\alpha} e^{\frac{\beta}{\alpha T}} \left(\text{erf} \sqrt{\frac{\alpha H_2 + \beta}{\alpha T}} - \text{erf} \sqrt{\frac{\alpha H_1 + \beta}{\alpha T}} \right) \right.$$
$$\left. - \frac{2}{\sqrt{\pi}} \left(\sqrt{\frac{\alpha H_2 + \beta}{T}} e^{-\frac{H_2}{T}} - \sqrt{\frac{\alpha H_1 + \beta}{T}} e^{-\frac{H_1}{T}} \right) \right]$$
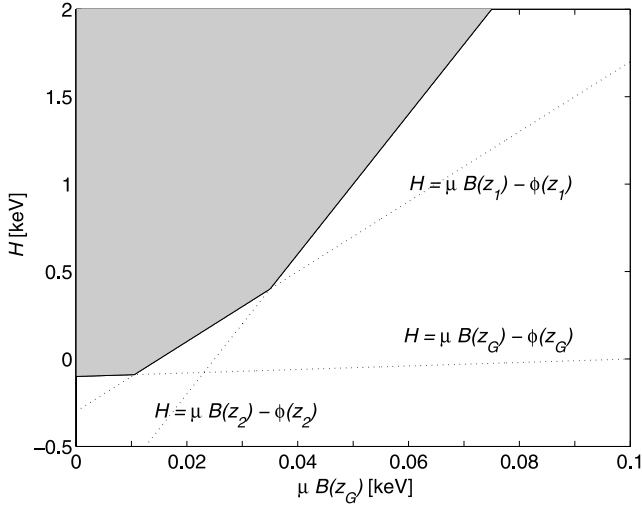$$(14)$$

Figure 1. Illustration to the first steps in the calculation of the integration boundary. The shaded area marks the region in the μ-H plane accessible to downgoing magnetospheric electrons. The points z_1 and z_2 are placed at $z_G + \Delta z$ and $z_G + 2\Delta z$, respectively.

where erf(z) is the error function. When the argument of the error function is imaginary, which happens when $\alpha < 0$, we use erf(iz) = i erfi(z) to write the result with only real numbers. In several cases $\mu_{max}(z, H)$ consists of only one or two line segments, and the densities are then given by reasonably simple expressions. For example, with the assumption made on the low-altitude potential in equation (9), the general expression for the ionospheric electron density is

$$
n_I(z) = \begin{cases}
\dfrac{N_F}{2} e^{-\frac{\phi_F}{T_F}} \left[e^{\frac{\phi}{T_F}} \text{erfc} \sqrt{\dfrac{\phi}{T_F}} \right. \\
\quad + \sqrt{1 - \dfrac{B}{B_0}} e^{\frac{\phi/T_F}{1-B/B_0}} \left(\text{erf} \sqrt{\dfrac{\phi/T_F}{1-B/B_0}} \right. \\
\quad \left. - \text{erf} \sqrt{\dfrac{\phi + \phi_F(B_0 - B)/(B_F - B_0)}{T_F(1 - B/B_0)}} \right) \\
\quad - \sqrt{1 - \dfrac{B}{B_F}} e^{\frac{\phi - \phi_F B/B_F}{T_F(1 - B/B_F)}} \\
\quad \left. \text{erfc} \sqrt{\dfrac{\phi + \phi_F(B_0 - B)/(B_F - B_0)}{T_F(1 - B/B_F)}} \right]; \qquad z \leq z_0 \\[2ex]
\dfrac{N_F}{2} e^{-\frac{\phi_F}{T_F}} \left[e^{\frac{\phi}{T_F}} \left(1 + \text{erf} \sqrt{\dfrac{\phi}{T_F}} \right) \right. \\
\quad - \sqrt{\dfrac{B}{B_0} - 1} e^{-\frac{\phi/T_F}{B/B_0 - 1}} \left(\text{erfi} \sqrt{\dfrac{\phi/T_F}{B/B_0 - 1}} \right. \\
\quad \left. - \text{erfi} \sqrt{\dfrac{\phi - \phi_F(B - B_0)/(B_F - B_0)}{T_F(B/B_0 - 1)}} \right) \\
\quad - \sqrt{1 - \dfrac{B}{B_F}} e^{\frac{\phi - \phi_F B/B_F}{T_F(1 - B/B_F)}} \\
\quad \left. \left(1 + \text{erf} \sqrt{\dfrac{\phi - \phi_F(B - B_0)/(B_F - B_0)}{T_F(1 - B/B_F)}} \right) \right]; \qquad z > z_0
\end{cases}
\tag{15}
$$

If we further assume that the magnetic field aligned electric field is positive for $z \leq z_0$, we obtain for the magnetospheric electron density

$$
n_M(z) = \begin{cases}
\dfrac{N_G}{2} e^{-\frac{\phi_G}{T_G}} \left[e^{\frac{\phi}{T_G}} \left(1 + \text{erf} \sqrt{\dfrac{\phi}{T_G}} \right) \right. \\
\quad - \sqrt{1 - \dfrac{B}{B_0}} e^{\frac{\phi/T_G}{1-B/B_0}} \left(\text{erf} \sqrt{\dfrac{\phi/T_G}{1-B/B_0}} \right. \\
\quad \left. - \text{erf} \sqrt{\dfrac{\phi + \phi_F(B_0 - B)/(B_F - B_0)}{T_G(1 - B/B_0)}} \right) \\
\quad + \sqrt{1 - \dfrac{B}{B_F}} e^{\frac{\phi - \phi_F B/B_F}{T_G(1 - B/B_F)}} \\
\quad \left. \text{erfc} \sqrt{\dfrac{\phi + \phi_F(B_0 - B)/(B_F - B_0)}{T_G(1 - B/B_F)}} \right]; \quad z \leq z_0 \\[2ex]
\dfrac{N_G}{2} e^{-\frac{\phi_G}{T_G}} \left[e^{\frac{\phi}{T_G}} \text{erfc} \sqrt{\dfrac{\phi}{T_G}} \right. \\
\quad + \sqrt{\dfrac{B}{B_0} - 1} e^{-\frac{\phi/T_G}{B/B_0 - 1}} \left(\text{erfi} \sqrt{\dfrac{\phi/T_G}{B/B_0 - 1}} \right. \\
\quad \left. + \text{erfi} \sqrt{\dfrac{\phi - \phi_F(B - B_0)/(B_F - B_0)}{T_G(B/B_0 - 1)}} \right) \\
\quad + \sqrt{1 - \dfrac{B}{B_F}} e^{\frac{\phi - \phi_F B/B_F}{T_G(1 - B/B_F)}} \\
\quad \left. \text{erfc} \sqrt{\dfrac{\phi - \phi_F(B - B_0)/(B_F - B_0)}{T_G(1 - B/B_F)}} \right]; \quad z > z_0
\end{cases}
\tag{16}
$$

The assumption that $\mu_{max}(z, H)$ is made up of at most two line segments is equivalent to assuming that the integration boundaries are completely determined by the local potential $\phi(z)$ and the potentials ϕ_F and ϕ_G at the boundaries. There is no reason to expect that this constraint should be respected by the potentials found in nature, but to simplify the calculations it has been assumed in many related studies [e.g., *Chiu and Schulz*, 1978; *Stern*, 1981; *Janhunen*, 1999; *Boström*, 2004]. The algorithm used in this study to calculate the densities allows $\mu_{max}(z, H)$ to consist of an arbitrary number of line segments and is valid for arbitrary shapes of the potential [*Vedin and Rönnmark*, 2004]. In practice it turns out that only the density of magnetospheric electrons in the region $z < z_0$ will be affected by the shape of the potential, and equations (15) and (16) will give the correct density in other cases.

4.2. Quasi-neutrality

[17] For a given $\phi_F < \Phi_a$, which closely corresponds to a given downward current, the equation for quasi-neutrality

$$
n_I(z) + n_M(z) = n_i(z)
\tag{17}
$$

involves three unknown variables, B_0, ϕ_G, and the local potential $\phi(z)$. However, by first solving the equation at the points z_0 and z_G, we eliminate the local potential, since it is equal to zero at one point and equal to ϕ_G at the other. At these points, the density is also independent of the potential shape. This implies that we have two equations, $n_I(z_0) + n_M(z_0) = n_i(z_0)$ and $n_I(z_G) + n_M(z_G) = n_i(z_G)$, that can be solved simultaneously for the two unknowns B_0 and ϕ_G by numerical iteration, using Newton's method.
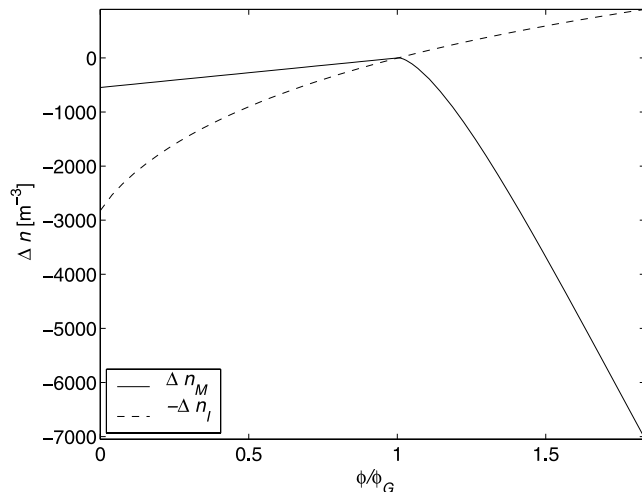
Figure 2. Electron density perturbations at $z_1 = z_G + 700$ km. Quasi-neutral solutions are found where the change Δn_M in the magnetospheric electron density (full line) equals the change $-\Delta n_I$ in the ionospheric electron density (dashed line). The potential is normalized to $\phi_G \approx 1$ V, and $j_F \approx 0.2$ μA/m^2.

[18] When using this method to solve for B_0 and ϕ_G, we find that ϕ_G raises as the current increases. At the generator boundary ($z = z_G$) the potential has little effect on the density of magnetospheric electrons, and we cannot reduce $n_M(z_G)$ to make room for more current carrying ionospheric electrons. To obtain a quasi-neutral solution at z_G, we must keep $n_I(z_G)$ constant by increasing ϕ_G in proportion to j_F^2. For current densities $j_F \lesssim 0.5$ μA/m^2 corresponding to $\phi_G \lesssim 5$ V, we find a quasi-neutral solution with $\phi(z_1) \approx \phi_G$ also inside the generator boundary at $z_1 = z_G + 700$ km where the magnetic field is $B_1 \approx 1.001 B_G$. To illustrate the nature of this solution, we show in Figure 2 the electron density perturbations $\Delta n_M = n_M - n_{Ma}$ and $-\Delta n_I = -(n_I - n_{Ia})$ as a functions of ϕ at z_1. A quasi-neutral solution, defined by $\Delta n_M + \Delta n_I = 0$, is found were the two curves cross. Increasing the current (reducing ϕ_F) slightly more, we can still find a quasi-neutral solution at z_G, but as illustrated in Figure 3 the solution at z_1 is now found at $\phi(z_1) \ll \phi_G$. If we increase the current further, $\phi(z_1)$ will go to zero and this solution will disappear. Since this type of solution implies that the potential is discontinuous at the boundary, we reject it as unphysical. Our conclusion is that the assumed boundary conditions, and in particular the constant N_G, are incompatible with downward currents $\gtrsim 0.5$ μA/m^2.

[19] Since the fixed N_G makes the problem overdetermined, we must relax the boundary conditions in order to obtain a well-posed problem. A natural choice is then to replace the constant N_G by a function $N_G(j_F)$ with $N_G(0) = 5 \times 10^5$ m^{-3} and determine $N_G(j_F)$ by extrapolating the density $n_M(z)$ from the interior of the flux tube to the boundary. To do this, we first, for each j_F, solve for B_0 and ϕ_G using $N_G(0)$. At z_1, inside the boundary, we then have the situation illustrated in Figure 3, indicating that the potential is discontinuous at the boundary. By comparing Δn_M with Δn_I at $\phi = 0.95\phi_G$, we then reduce $N_G(j_F)$ until we reach the situation shown in Figure 4, which illustrates the density variations at z_1 when $N_G(j_F)$ has been reduced just

enough to be compatible with the given current. We see that the curve Δn_M then becomes tangential to $-\Delta n_I$ as ϕ approaches ϕ_G from below, which indicates that the potential jump from $\phi(z_1)$ to ϕ_G at the boundary is vanishingly small. By reducing $N_G(j_F)$ in steps of $10^{-4} N_G(0)$, we locate in this way the largest $N_G(j_F)$ consistent with a continuous potential and density at the generator boundary.

[20] To find the shape of the potential along the rest of the field line, we first notice that all ionospheric electrons that pass the potential minimum at z_0 will continue up to the generator. Hence the density of ionospheric electrons at a particular $z = z_k$ depends on ϕ_F, B_0, and $\phi(z_k)$ but not on the potential at any other $z \neq z_k$. This implies that we can use equation (15) for the ionospheric electron density. The density of the magnetospheric electrons, on the other hand, depends on the shape of the potential at $z < z_k$, since it affects the number of electrons mirroring above z_k. However, the density at z_k is independent of the shape of $\phi(z)$ for $z > z_k$. Hence knowing ϕ_F, B_0, and ϕ_G, we can guess a $\phi(z_1)$, calculate the total electron density at $z_1 = z_G + \Delta z$ and iterate until we find a $\phi(z_1)$ that gives quasi-neutrality. Knowing $\phi(z_j)$ for $j \leq k$, we can determine $\mu_{max}(z_{k+1}, H)$, calculate the densities at z_{k+1}, and iterate to find $\phi(z_{k+1})$ in a similar way, without disturbing the densities at higher altitudes. Repeating these steps for each k until we reach z_F, we have found a potential that is consistent with quasi-neutrality all along the field line.

4.3. Model Parameters

[21] All results in this study are based on a single set of model parameters. The flux tube has a length of $L_z = 5.5 \times 10^4$ km (or 8.6 R_E). We use a nonuniform grid with 200 grid points, and Δz is decreasing from 700 km near the generator to 70 km in the ionosphere. In the results we will also use the height $h = L_z - z$ above the ionospheric boundary. The height where the ambipolar potential $\Phi(z)$ goes to zero is chosen to be $h_a \approx 2.5 \times 10^3$ km, and equation (6) then gives $\Phi_a \approx 9.7$ V.
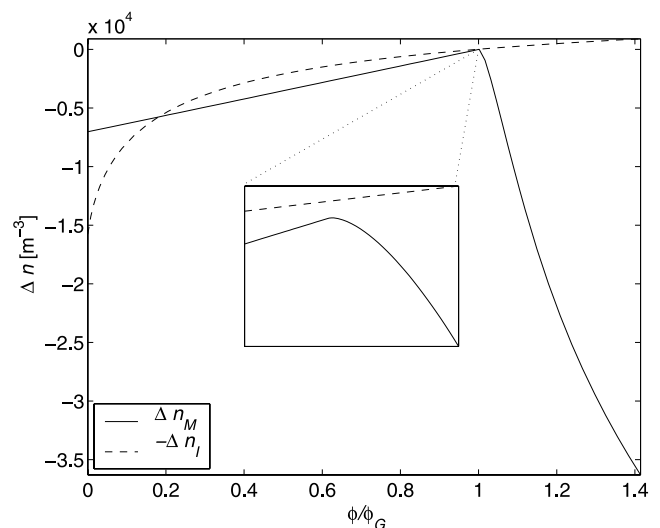

Figure 3. The electron density perturbations at z_1 when the current is $j_F \approx 1.1$ μA/m^2. There is no solution at $\phi \approx \phi_G$ in this case, as can be seen in the inserted box. The potential is normalized to $\phi_G \approx 14$ V.
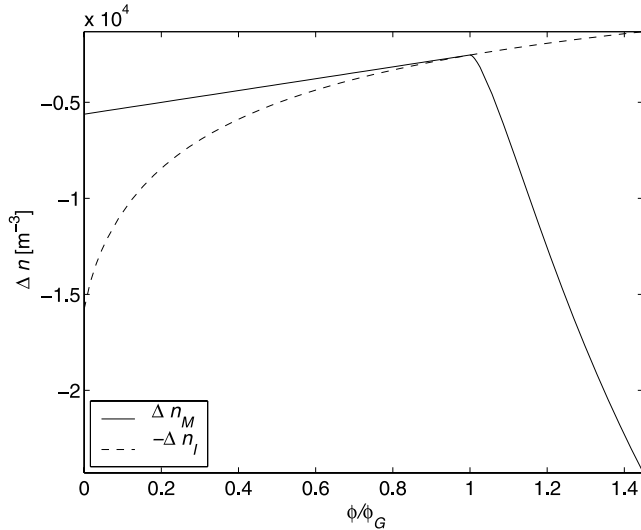
Figure 4. This figure shows the same situation as Figure 3, but here $N_G(j_F)$ has been reduced just enough to give a continuous potential at the generator boundary. The boundary potential is then reduced to $\phi_G \approx 4$ V.

[22] The geomagnetic field strength is modeled by

$$B(z) = B_G \exp\left[(z/L_z)^2 (\ln(B_F/B_G) - 0.6 - 1.8(z/L_z)^2 + 2.4(z/L_z)^6)\right], \quad (18)$$

with an ionospheric field strength $B_F = 56$ μT, and $B_G = 0.0864$ μT at the generator boundary. This magnetic field model approximates the dipole field for the $L = 7$ shell. All numerical values for the current density presented in the results will be mapped to the ionospheric boundary and are therefore denoted j_F.

5. Results

[23] As we have described above, the strategy in this study is to start from a current-free state with an ambipolar potential $\Phi(z)$, and by reducing the ionospheric potential ϕ_F in steps we then increase the current. Figure 5a shows the relation between ϕ_F and the field-aligned current density j_F. Notice that as long as the minimum potential along the field line is $\phi = 0$, the current is almost completely determined by ϕ_F. Adjustments of the electron densities, required for quasi-neutrality, can be done by varying the shape of the potential within the rest of the flux tube without significantly altering the current. A reduction of the upward electric field at low altitudes would not be consistent with quasi-neutrality, and the decrease in ϕ_F is mainly due to a reduction of the altitude h_0 where the potential becomes zero. As shown in Figure 5b, the altitude h_0 of the global minimum in the potential is halved from $h_a = 2.5 \times 10^3$ km to $h_0 \sim 1.3 \times 10^3$ km when the current increases. If the potential minimum initially is higher, at $h_a = 5.5 \times 10^3$ km, the reduction of h_0 is even stronger as shown by the dashed curve. On longer timescales we expect the outflow of heated ions to create a cavity in the ionospheric density, and this will of course affect the profile of the potential near its minimum.

[24] Figure 6 illustrates how the shape of the self-consistent potential varies with the current density. At low current densities there is a rather broad maximum in the potential, with a plateau at altitudes between $\sim$0.5 R_E and $\sim$3 R_E. When the current is about 5 μA/m^2 and the potential has increased to around 200 V, a peak starts to develop in the potential at around 2 R_E. As the current grows, this peak moves to lower altitudes and grows in magnitude. At a current density of 25 μA/m^2, the peak potential is $\sim$2.5 kV at an altitude near 0.7 R_E. While the downward electric field is weak and extends over $\sim$2 R_E, the downward field is sharply peaked just above z_0. The peak downward electric field reaches more than 5 mV/m when $j_F = 20$ μA/m^2.

[25] The qualitative features of the potential are not very sensitive to variations in the model parameters. If we increase the height of the initial ambipolar electric field to $h_a = 5.5 \times 10^3$ km, the only major change in the results, apart from the increase in h_0 shown in Figure 5b, is that the potential maximum is reduced by $\sim$30% compared with the results presented in Figure 6. The general shape of the potential is rather unaffected by variations of the magnetospheric electron density and temperature. At least for $j_F < 10$ μA/m^2 there is little change in ϕ_{max} if $N_G(0)T_G^{1/2}$ is kept constant while $N_G(0)$ is increased or reduced by a factor of two. However, the magnitude of ϕ_{max} is reduced if $N_G(0)$ or T_G is independently increased. This can be understood by noticing that according to equation (4) the current carried by magnetospheric electrons increases in proportion to $N_G(0)v_G$. To compensate for this upward current, the ambipolar potential must be reduced to increase the current carried by ionospheric electrons in the initial state. A larger ionospheric current in the ground state implies that a specific increase in the total downward current density can be accomplished by smaller deviations from the initial potential profile. At higher current densities, producing ϕ_{max} T_G, we find that the combination $N_G(0) = 2.5 \cdot 10^5$ m^{-3}, $T_G = 4$ keV leads to somewhat higher potentials than $N_G(0) = 10^6$ m^{-3}, $T_G = 250$ eV.
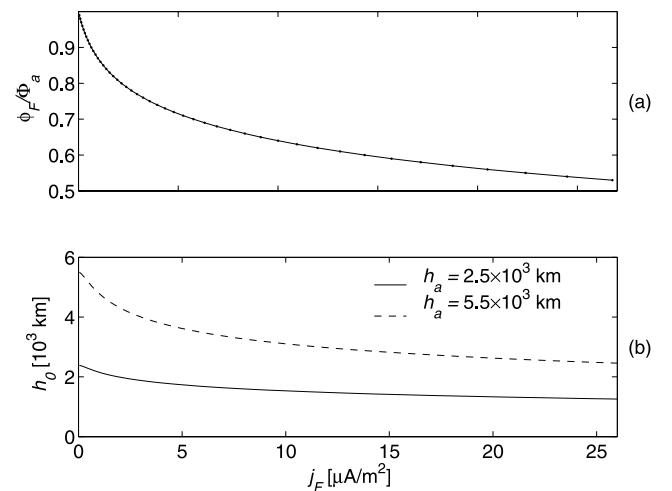

Figure 5. The dependence of (a) the ionospheric potential and (b) the altitude of the potential minimum on the current density. In Figure 5b, the solid line corresponds to an initial height $h_a = 2.5 \times 10^3$ km, and the dashed line corresponds to $h_a = 5.5 \times 10^3$ km.
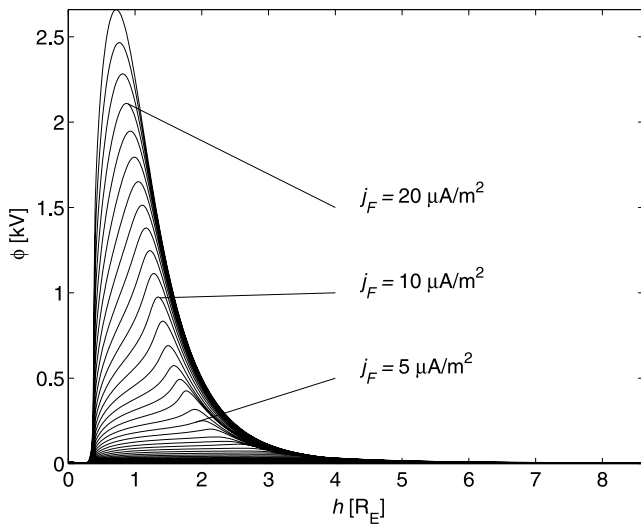
Figure 6. The potential profile $\phi(z)$ at different current densities varying from 0 μA/m^2 to 25 μA/m^2. The different profiles correspond to the dots on the curve in Figure 5a.

[26] The altitude of the potential peak coincides with the minimum of n_I/B, shown by the dotted line in Figure 7. Since current conservation implies that the drift velocity of the ionospheric electrons must be proportional to B/n_I, their velocity, as well as the potential, will have a maximum at this altitude. Above the potential peak, n_I/B increases and the drift velocity decreases. When they arrive at the generator boundary, the drift velocity of the ionospheric electrons is comparable to their thermal velocity. Figure 7 also shows that the magnetospheric electron density is reduced as required to make room for the current carrying ionospheric electrons.

[27] At low current densities, below $\sim$0.5 μA/m^2, quasi-neutrality at the generator boundary can be maintained by increasing ϕ_G, thus increasing the velocity of ionospheric

electrons and reducing their density. For these currents we find solutions with a potential that decreases monotonically between z_G and z_0. However, by raising the mirror points, increasing ϕ_G also causes an increase of n_M at high altitudes, and for $\phi_G \gtrsim 5$ V this effect dominates the reduction of n_I. Quasi-neutrality can then no longer be maintained by further increasing ϕ_G. To allow strong currents, we must reduce N_G, as shown in Figure 8a, to maintain quasi-neutrality at the generator boundary. The consequences of this reduction of N_G can be seen in Figure 8b. The potential ϕ_G at the generator boundary increases rapidly to $\sim$5 V while we keep N_G fixed, but when we start to reduce N_G the generator potential slowly drops down to $\lesssim$0.2 V.

[28] Figure 8c shows how the maximum value of the potential, ϕ_{max}, increases with increasing current. When we drive current densities of more than $\sim$10 μA/m^2 through the flux tube, ϕ_{max} is greater than about 1 kV and increases linearly in proportion to the current.

6. Discussion

[29] Earlier models of the downward auroral current region have only described the lower [*Jasperse*, 1998; *Jasperse and Grossbard*, 2000] or upper [*Temerin and Carlson*, 1998] part of the flux tube. It is difficult to compare our model of the lower part of the flux tube with those of *Jasperse* [1998] and *Jasperse and Grossbard* [2000], since we focus on the variations of the current and potential and neglect wave-particle interactions. The lower boundary of the *Temerin and Carlson* [1998] model is at a point where the ambipolar electric field goes to zero, corresponding to our h_a, while our model continues seamlessly down to the ionospheric F layer. Still, since *Temerin and Carlson* [1998] consider current variations and neglect wave-particle interactions, our model is more comparable to theirs.

[30] While we keep the ion density fixed everywhere and determine a potential that maintains quasi-neutrality all the way down to the F layer, *Temerin and Carlson* [1998] increase the ion density at and slightly above h_a
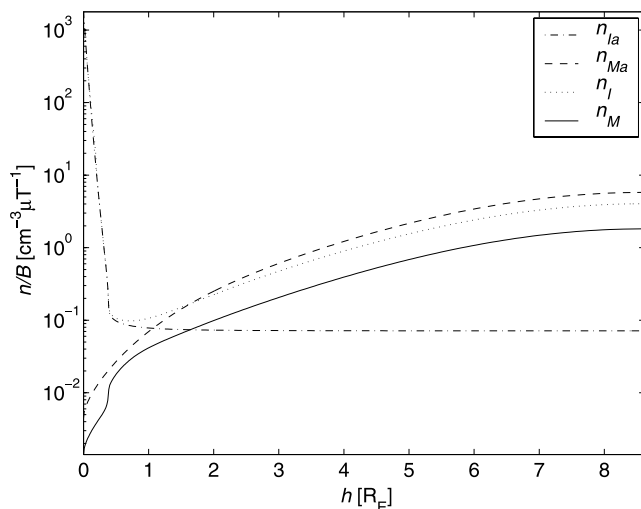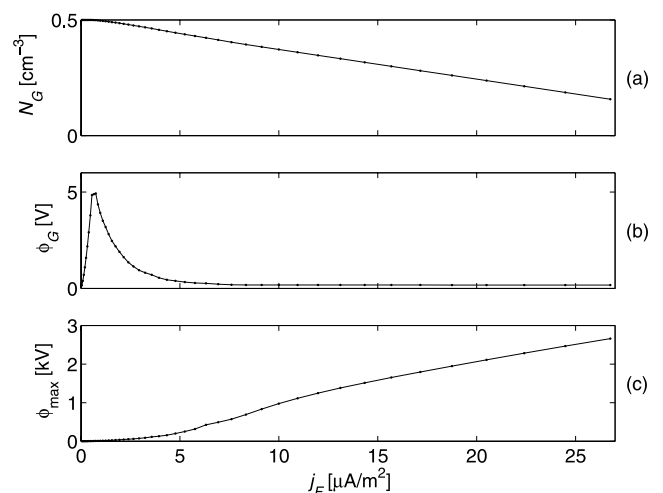

Figure 7. The density profiles n_{Ia}/B and n_{Ma}/B in the current-free state compared with the corresponding density profiles n_I/B and n_M/B in the state with a current density of 25 μA/m^2.

Figure 8. The dependence of (a) $N_G(j_F)$, (b) the generator boundary potential ϕ_G, and (c) the maximum the potential ϕ_{max} on the current density.

($\sim$3000 km) to allow the current to increase. We find this increase of the plasma density at an altitude where we expect density cavities to form less attractive. In our model we instead make more ionospheric electrons available for upward acceleration by lowering the altitude h_0 of the potential minimum into the dense ionospheric plasma. In both models, the density of magnetospheric electrons is also reduced, in order to make room for the current-carrying ionospheric electrons.

[31] With the fixed, rather smooth, density profile used in this study, we find downward field-aligned electric fields of 5 mV/m in a narrow region just above h_0. As discussed in section 1, our model should apply to timescales shorter than $\tau_i \sim 100$ s on which changes in the ion density become significant. On a longer timescale it seems likely that electrostatic forces as well as ion heating will create a plasma cavity at altitudes near the potential peak. This could start a feedback loop, where a steeper density gradient at the low-altitude end of the cavity leads to even larger downward electric fields. Such processes are outside the scope of this study, but we emphasize that although the ion density is held fixed in our model, its evolution can significantly alter the potential on longer timescales. Remember that we in section 1 discussed the timescales for which this model is valid in a more quantitatively way.

[32] In a stationary model there is no unique way to introduce a population of trapped electrons, and this is therefore not done in the model presented here. Trapped electrons can affect the quasi-neutral potential without changing the current density and could therefore alter our results. The ideas in this study should be considered as a first simplified step toward the understanding of the return current region and a natural step toward a more realistic model would be to include trapped electrons. However, as we will discuss later in this section, an even more important step in improving this model would be to include wave-particle scattering. The phase space diffusion from such scattering would unambiguously define a density of trapped electrons.

[33] A potential with a peak $\gtrsim 1$ kV at altitudes around 1 R_E can in a natural way explain the simultaneous occurrence of ion conics elevated by several hundred eV and beams of upgoing electrons accelerated to similar energies observed by the Viking satellite at altitudes near 2 R_E [*Hultqvist et al.*, 1988]. In the "pressure cooker" [*Lynch et al.*, 2002; *Gorney et al.*, 1985] below the potential peak, ions are kept down by the downward electric field while they are perpendicularly heated by low-frequency waves. The heated ions will form a conic distribution when they have gained enough energy to climb the potential peak, and the apex of the cone will be elevated in parallel energy by the upward electric field above the peak. At altitudes around 2 R_E the ion conic is elevated by several hundred eV, and the current-carrying, upgoing, ionospheric electrons still have parallel energies of a few hundred eV. Hence our model provides a very simple explanation for the Viking observations.

[34] An important result of this study is that the density parameter N_G cannot be held constant when the current varies. Although the assumption of constant N_G was reasonable in studies such as *Knight* [1973], it is not compatible with the requirement of quasi-neutrality [see, e.g., *Jasperse and Grossbard*, 2000]. This conclusion applies also to the upward current region. An increase of the ionospheric potential, corresponding to a higher upward current density, would reduce the densities of both magnetospheric and ionospheric electrons just below the generator boundary. If the ion density remains constant, this would create a positive space charge. Notice that the need to adjust N_G remains if we assume also the ions to adjust to changes in the potential, since the changes in the ion density in general will be opposite to the changes in the electron density.

[35] *Temerin and Carlson* [1998] avoid the boundary discontinuity that forces us to reduce N_G by letting $B \rightarrow 0$ at the upper boundary of the flux tube. This implies that at the boundary n_I becomes negligible for any finite current and allows them to keep N_G constant. They also approximate the density of magnetospheric electrons by $n_M(z) = N_G \exp[e(\phi_G - \phi)/T_G]$, thus neglecting the effects of the loss cone. These differences in the boundary conditions and density calculations are probably the main reasons why Temerin-Carlson with fixed N_G find solutions where ϕ_G increases with the current, while we are forced to reduce N_G and thus obtain solutions with $\phi_G \lesssim 5$ V.

[36] A quantitative discussion of the processes within the generator that are responsible for adjusting the boundary conditions is beyond the scope of this study. However, it may be noticed that a field-aligned current $j_F \sim 10$ μA/m^2 corresponds to an electron flux of 10^{11} m^{-2}s^{-1} at the generator. If this flux cannot be supplied by ionospheric electrons, the density of magnetospheric electrons will be reduced at a rate $\sim$3%/s over an altitude range of 1 R_E. At lower altitudes, where the flux tube is narrower, the depletion of magnetospheric electrons will be proportionally faster. Ionospheric electrons will then flow up to maintain quasi-neutrality, until the quasi-stationary equilibrium we consider has been established. In practice there can be alternative adjustments, such as increasing the ion density, which also may allow strong downward currents to connect to the generator.

[37] In the absence of wave-particle interactions, the beams resulting from electrostatic acceleration of low-energy ionospheric electrons should be essentially mono-energetic. However, such cold beams are unstable and will rapidly generate waves, which will scatter the electrons. While the energy spectrum of the downward accelerated electrons in auroral arcs usually has a clear lower cutoff, the spectrum of upgoing electron beams extends from low energies to an upper cutoff that corresponds to the electrostatic potential. This is consistent with strong wave-particle scattering and suggests that results derived from the adiabatic electron trajectories may be significantly modified by wave-particle interactions in the downward current region. Recent observations [*Marklund et al.*, 2001; *Johansson et al.*, 2004] of upgoing electron beams with keV energies by the Cluster satellites at altitudes near 4 R_E indicate that the positive potential extends to higher altitudes than predicted by our model. However, the adiabatic model used in this study should be regarded as a lowest-order approximation, and wave-particle scattering must be taken into account when comparing our results with observations. For example, scattering of current-carrying ionospheric electrons to lower energies will reduce the downward current. It seems likely that in order to maintain the current, such scattering

will require a larger downward electric field below the potential peak and a weaker upward electric above the peak. This could result in an enhancement of the potential, particularly at higher altitudes.

References

Andersson, L., R. E. Ergun, D. L. Newman, J. P. McFadden, C. W. Carlson, and Y.-J. Su (2002), Characteristics of parallel electric fields in the downward current region of the aurora, *Phys. Plasmas*, *9*, 3600.

Boström, R. (2004), Kinetic and space charge control of current flow and voltage drops along magnetic flux tubes: 2. Space charge effects, *J. Geophys. Res.*, *109*, A01208, doi:10.1029/2003JA010078.

Chiu, Y. T., and M. Schulz (1978), Self-consistent particle and parallel electrostatic field distribution in the magnetospheric-ionospheric auroral region, *J. Geophys. Res.*, *83*, 629–642.

Goertz, C. K., and R. W. Boswell (1979), Magnetosphere-ionosphere coupling, *J. Geophys. Res.*, *84*, 7239–7246.

Gorney, D. J., Y. T. Chiu, and D. R. Croley (1985), Trapping of ion conics by downward parallel electric fields, *J. Geophys. Res.*, *90*, 4205–4210.

Hultqvist, B., R. Lundin, K. Stasiewicz, L. Block, P.-A. Lindqvist, G. Gustafsson, H. Koskinen, A. Bahnsen, T. A. Potemra, and L. J. Zanetti (1988), Simultaneous observations of upward moving field-aligned energetic electrons and ions on auroral zone field lines, *J. Geophys. Res.*, *93*, 9765–9776.

Janhunen, P. (1999), On the current-voltage relationship in fluid theory, *Ann. Geophys.*, *17*, 11–26.

Jasperse, J. R. (1998), Ion heating, electron acceleration, and the self-consistent parallel E-field in downward auroral current regions, *Geophys. Res. Lett.*, *25*, 3485.

Jasperse, J. R., and N. J. Grossbard (2000), The Alfvén-Fälthammar formula for the parallel E-field and its analogue in downward auroral-aurrent regions, *IEEE Trans. Plasma Sci.*, *28*, 1874.

Johansson, T., S. Figueiredo, T. Karlsson, G. Marklund, A. Fazakerley, S. Buchert, P.-A. Lindqvist, and H. Nilsson (2004), Intense high-altitude auroral electric fields—Temporal and spatial characteristics, *Ann. Geophys.*, *22*, 2485–2495.

Knight, S. (1973), Parallel electric fields, *Planet. Space Sci.*, *21*, 741–750.

Lynch, K. A., J. W. Bonnell, C. W. Carlson, and W. J. Peria (2002), Return current region aurora: $E_\parallel$, j_z particle energization and broadband ELF wave activity, *J. Geophys. Res.*, *107*(A7), 1115, doi:10.1029/2001JA900134.

Lysak, R. L., and C. Dum (1983), Dynamics of magnetosphere-ionosphere coupling including turbulent transport, *J. Geophys. Res.*, *88*, 365–380.

Lysak, R. L., and Y. Song (2003), Nonlocal kinetic theory of the Alfvén waves on dipolar field lines, *J. Geophys. Res.*, *108*(A8), 1327, doi:10.1029/2003JA009859.

Marklund, G. T., and T. Karlsson (2001), Characteristics of the auroral particle acceleration in the upward and downward current regions, *Phys. Chem. Earth*, *26*, 81–96.

Marklund, G. T., et al. (2001), Temporal evolution of the electric field accelerating electrons away from the auroral ionosphere, *Nature*, *414*, 724–727.

Rönnmark, K., and M. Hamrin (2000), Auroral electron acceleration by Alfvén waves and electrostatic fields, *J. Geophys. Res.*, *105*, 25,333–25,344.

Stern, D. P. (1981), One-dimensional models of quasi-neutral parallel electric fields, *J. Geophys. Res.*, *86*, 5839–5860.

Streltsov, A. V., W. Lotko, J. R. Johnson, and C. Z. Cheng (1998), Small-scale, dispersive field line resonances in the hot magnetospheric plasma, *J. Geophys. Res.*, *103*, 26,559–26,572.

Temerin, M., and C. W. Carlson (1998), Current-voltage relationship in the downward auroral current region, *Geophys. Res. Lett.*, *25*, 2365–2368.

Tikhonchuk, V. T., and R. Rankin (2000), Electron kinetic effects in standing shear Alfvén waves in the dipolar magnetosphere, *Phys. Plasmas*, *7*(6), 2630–2645.

Tikhonchuk, V. T., and R. Rankin (2002), Parallel potential driven by a kinetic Alfvén wave on geomagnetic field lines, *J. Geophys. Res.*, *107*(A7), 1104, doi:10.1029/2001JA000231.

Vedin, J., and K. Rönnmark (2004), A linear auroral current-voltage relation in fluid theory, *Ann. Geophys.*, *22*, 1719–1728.

Vedin, J., and K. Rönnmark (2005), Electron pressure effects on driven auroral Alfvén waves, *J. Geophys. Res.*, *110*, A01214, doi:10.1029/2004JA010610.

_____

K. Rönnmark and J. Vedin, Department of Physics, Umeå University, SE-901 87 Umeå, Sweden. (kjell.ronnmark@space.umu.se; jorgen.vedin@space.umu.se)